OPEN ACCESS
JOURNAL OF ADVANCED DIELECTRICS
2350029 (11 pages)

DOI: 10.1142/S2010135X23500297

Dual nitrogen-sulfur-doping induce microwave absorption and EMI shielding in nanocomposites based on graphene

Tienah H. H. Elagib *,†,§, Nassereldeen A. Kabbashi *, Md Zahangir Alam *, Elwathig A. M. Hassan *, Mohamed E. S. Mirghani * and Nour Hamid Abdurahman ‡

*Department of Chemical Engineering and Sustainability
International Islamic University Malaysia
Jalan Gombak 53100, Kuala Lumpur, Malaysia

†Department of Materials Engineering, University of Gezira
Address Wad Madani, Gezira State 21111, Sudan

‡Faculty of Chemical and Process Engineering Technology
Universiti Malaysia Pahang Al-Sultan Abdullah
26660 Pahang, Malaysia

§tienahhussain25024@gmail.com

Received 15 October 2023; Revised 26 November 2023; Accepted 29 November 2023; Published 21 December 2023

Graphene-oxide (GO) is one of the most commonly used carbon nanomaterials in advanced applications such as microwave absorption and EMI shielding, due to various advantages such as ease of synthesis and exfoliation, effective doping capability, and superior composite compatibility. In this study, we used the modified Hummer's method to synthesize GO by exfoliating graphite powder, and a simple hydrothermal approach was employed for elemental doping and GO reduction. As nitrogen–sulfur (N, S) dual-doping precursors, thiourea and l-cysteine amino acids were utilized. The structural features and microporous network structure of GO aerogel foams were investigated. The microwave absorption capabilities of polyethersulfone-based nanocomposite films incorporating the as-produced nitrogen–sulfur enrich reduced GO (NS-rGO) are also explored. According to the physico-chemical characterization, the existence of remarkable structural defects with a porous three-dimensional (3D) network was discovered due to heteroatom insertion and hydrothermal doping. Additionally, the dual-doped sample exhibited high Nitrogen and sulfur content of 8.93% and 13.19%, respectively. While NS-rGO possesses a higher conductivity of 174.7 μS compared to 12.65 μS for GO. The nanocomposites filled with NS-rGO foams demonstrated a high shielding efficiency (SE) of 45 dB in the X-band with a filler loading of 0.5 wt.%. This high SE arises from dopant heteroatoms and the heterogeneous interface, which induce interface polarization, thereby increasing microwave absorption and dielectric constant. It also results from multi-level reflections caused by the 3D porous structures. These findings offer valuable insights into the functionalization of carbon nanostructures and the development of 3D networks in GO-based functional materials, providing further guidance for engineering high-performance electromagnetic interference shielding materials.

Keywords: Shielding performance; multi-level reflection; hydrothermal synthesis; porous structure.

1. Introduction

In response to the escalating problem of electromagnetic (EM) pollution, a considerable amount of attention has been directed toward the field of advanced functional materials[1] for the design and development of microwave absorption materials.[2,3] Among these materials, polymer composites could be considered a promising choice for addressing the electromagnetic interference (EMI) problem.[4,5] Their anti-corrosion properties, light weight, flexibility, and ease of processing make them beneficial for this purpose.[6]

In EMI shielding applications, nanocomposites based on generic polymers filled with carbonaceous materials such as carbon nanotubes (CNTs),[7] carbon black,[8] carbon fiber,[9] and two-dimensional (2D) transition metal nitride/ carbide /carbonitrides (MXene),[10] graphene,[11] and graphene oxide (GO)[12] have an advantage over rigid, metal-based shielding materials.

These conductive/carbonaceous fillers mitigate EMI by reflecting and absorbing EM waves through dielectric relaxation and conduction losses.[13] Carbonaceous nano-structured materials, in general, are used as fillers in polymeric matrices due to their low density, high conductivity, thermal stability, high permittivity, and controllable aspect ratio.[14] The polymer matrix plays two key roles in EMI shielding; it provides flexibility and mechanical strength to the EMI shielding layer and allows incoming EM waves to

§Corresponding author.

pass through the shielding layer because polymers often exhibit transparency toward high-frequency EM waves.[15]

According to Sushmita and co-workers, the introduction of structural defects in CNTs and the utilization of suitable functional groups that can enhance interactions with the host polymer play significant roles in improving shielding performance.[16] CNTs are preferred because of their low cost, small diameter, ease of percolation, excellent electrical conductivity, and high mechanical strength.[17] Another study found that covalent bonding between a polyaniline matrix and graphene aerogel fillers enhances electron transfer, effectively converting EM energy into heat energy, thereby improving microwave absorption capacity.[18] Due to their exceptional electron mobility (15,000 $cm^2V^{-1}s^{-1}$), large aspect ratios, high thermal conductivity (5000 Wm^{-1} K^{-1}), tunable electrical properties, abundance of functional groups, and excellent mechanical characteristics, 2D graphene materials have emerged as popular alternatives for EMI shielding.[19] However, the irreversible aggregation of graphene can significantly diminish its intrinsically high electrical conductivity. Fortunately, the problem of graphene agglomeration can be successfully addressed by using three-dimensional (3D) networks.[20]

Recently, a variety of micro-structural designs of filler including segregate structures,[21,22] porous structures,[23,24] and multi-layer structures[25,26] have been reported in the literature achieving valuable EMI shielding performance with low filler loading. Researchers have increasingly focused on fabricating porous structures of carbonaceous materials, such as foams[27] or aerogel,[18] due to their lightweight, high specific surface area, and high dielectric loss.[28,29] Generally speaking, various methods have been proposed to introduce porous structures, including chemical foaming,[30] freeze-drying,[18] and supercritical carbon dioxide ($scCO_2$) foaming[31] among others. For instance, Thomassin *et al.* used $scCO_2$ to foam polycaprolactone (PCL)/MWNTs composites, resulting in a shielding efficiency of (60–80) dB with low reflectivity at low MWNTs loading of 0.25 vol.%.[32] In a different technique, Wang *et al.*[33] employed a new type of carbon tube with a whisker structure and excellent electrical conductivity. They used GO as a bridging and foaming agent to achieve a porous film via a vacuum-assisted filtration and annealing process. This yielded a remarkable near-field shielding performance of 25–50 dB in the frequency range of 1–9 GH. This confirmed that the porous structures induced by GO during the thermal reduction process changed the polarization direction and distribution of the electric field of attenuated EM waves. However, graphene's excess dielectric constants limit its ability to achieve appropriate impedance matching. One approach to overcome this issue is to dope heteroatoms into graphene materials, thereby introducing significant structural defects and inducing extra polarization relaxation.[34] Dopant atoms, in fact, introduce charge into the electron system of sp2-bonded carbon materials.[35] Because of the presence of these dopant atoms, free charges become trapped by defects caused by doping under EM fields, leading to an asymmetric distribution of charges around these defects. When exposed to an alternating EM field, these defects frequently act as polarization centers, resulting in polarization relaxation. Notably, the defective sites serve as permanent dipolar polarization centers, resulting in additional dielectric polarization.[36]

It can be argued that heteroatom doping is a commonly used method to adjust electronic structure and other material characteristics. It serves three main functions: (1) it increases the number of polarizing centers, (2) it tunes the bandgap, and (3) it enhances dielectric properties.[37] Therefore, may assist in improving the performance of graphene for particular applications. Nitrogen (N) is often used as a doping element because it can strengthen EM attenuation capacity due to dielectric loss, lower electrical conductivity, enhance the magnetization performance,[38] and enhance the multiple scatterings as well as the balanced impedance match.[39] In fact, the size of the N atom is very similar to that of a carbon (C) atom, and it has five valence electrons, which can easily bond with C atoms.[37] Furthermore, the difference in electronegativity between the C atom (2.55) and the N atom (3.04) disrupts the electro-neutrality of graphene material and causes the change in atomic charge distribution and spin density. These changes may serve as the source of the magnetic property of graphene.[40] On the other hand, introducing sulfur (S) into a graphene sheet can improve its magnetic characteristics. As S has two additional electrons, incorporating these two unpaired electrons by each S atom into the conducting band — where they become delocalized among the S and C atoms,— can enhance the magnetic properties.[41]

As reported in the literature, the development of nitrogen-doped graphene composites for the purpose of microwave absorption enhancement was achieved very successfully.[42,43] Besides, there are numerous studies related to the dual doping of graphitic materials with the S and the N which potentially possess promising properties for various applications.[44–47] However, there remains a dearth of research on the effect of the N and the S dual-doping of graphene or GO and their composites on EMI shielding performance. Therefore, this work focuses on studying how heteroatom doping affects dielectric properties and EMI shielding effectiveness (SE) of N-co-S enrich reduced graphene oxide (rGO) filled polymer nanocomposites. Herein, we employed a simple functionalization technique for inserting heteroatoms into the surface of GO followed by a hot-pressing method to fabricate the shielding nanocomposite film. These techniques were chosen in an attempt to overcome challenges in manufacturing shielding materials, such as complicated preparation processes, high costs, and environmental harm.

2. Experimental Results

2.1. *Materials*

The graphite powder used in this study was supplied by Zen Chemicals, while the polyethersulfone (PES) was purchased

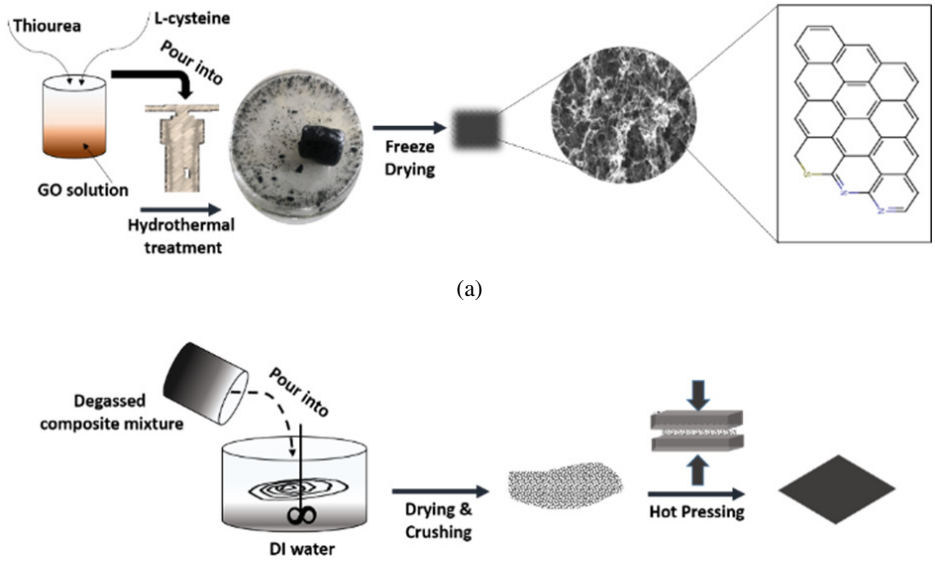

Fig. 1. Schematic illustration of (a) the synthesis procedure of the dual doping of rGO foams and (b) the fabrication of nanocomposite film.

from BASF, Ludwigshafen, Germany. Multiwall carbon nanotubes (MWCNTs) were provided by Sigma Aldrich. The l-cysteine (L-Cys) was purchased from Beijing Solarbio Science & Technology. Thiourea (with a purity greater than 98%), N, N-Dimethyleformamide (DMF), and sulfuric acid (H_2SO_4) with a purity of about 98% were supplied by R&M Chemicals. Sodium nitrate ($NaNO_3$) with a purity greater than 98%, was also obtained from the same supplier. Hydrogen peroxide (H_2O_2) was provided by Bendosen Laboratory Chemicals, while potassium permanganate ($KMNO_4$) with a purity greater than 99% was supplied by Chemiz (M) Sdn. Bhd.

2.2. *Preparation of graphene oxide*

GO was prepared by chemical exfoliation of graphite powder according to a modified Hummer's method. In a typical process, 2 g graphite power was dispersed in 46 ml H_2SO_4 and 1 g $NaNO_3$. The mixture was then placed into an ice bath (0–5°C) under continuous stirring. 6 g $KMNO_4$ was added into the mixture portion-wise, and the reaction was kept for at least 2 h and then maintained below 15°C, (the color became green). The ice bath was removed, and the reaction was kept under stirring for 2–3 h at 35°C (the color altered to dark green). After that, 100 ml deionized (di)-water was added and the reaction was maintained at 90–98°C (the color changed to yellowish brown), and the reaction was kept under this temperature for 30 min, then another 200 ml di-water was added portion wise under stirring. The temperature was decreased to 70°C and then 20 ml H_2O_2 (30 wt.%) was added into the solution. GO was obtained after centrifugation at 7000 rpm.

2.3. *Synthesis of N, S dual-doped rGO foams*

In a typical process as described in Fig. 1(a), 0.2 g GO was dispersed by ultra-sonication in 100 ml of deionized water for 2 h. In contrast, 0.30 g of a 1:1 mixture of L-Cys and thiourea was dispersed by ultra-sonication in 30 ml of the GO dispersion. The mixture was then transferred into an autoclave with a Teflon liner for hydrothermal treatment lasting 16 h at 170°C. The temperature was maintained at approximately 170°C for the duration of the treatment. Following this, the resulting product was thoroughly rinsed with di-water and then freeze-dried. The resulting nitrogen and sulfur-enriched rGO foam was denoted as NS-rGO. Oxidized CNT was prepared from neat CNTs in our lab as mentioned in our previous work.[46] Nitrogen and sulfur dual-doped oxidized CNT (NS-OCNT) was prepared under the same hydrothermal conditions.

2.4. *Nanocomposite fabrication*

Figure 1(b) illustrates the preparation procedure of the nanocomposite samples. Typically, PES and NS-rGO foams were dissolved separately in DMF by ultra-sonication before being mixed together to form the composite mixture. Then, the mixture was degassed for 30 min and slowly poured into di-water under mild stirring. It was then dried at 80°C for 48 h. The dried NS-rGO/PES nanocomposite was crushed into small pieces using a crushing machine. The fabrication of nanocomposite film was performed by a tablet pressing machine (XH-406B) under a pressure of 15 MPa for 10 min at 180°C. The resulting nanocomposite films, which had a thickness of 3 mm, were denoted as follows: GO@PES1 (Control sample, with 0.2 wt.% GO loading), NS-rGO@PES2

(with 0.2 wt.% NS-rGO loading), NS-rGO@PES3 (with 0.5 wt.% NS-rGO loading). For comparison, a nanocomposite with 0.5 wt.% NS-OCNT loading was also prepared and named NS-OCNT@PES4.

2.5. *Measurements*

The phase patterns of the doped samples were examined using an X-ray diffractometer (XRD) (D2 PHASER – Bruker, Germany) with Cu Kα radiation, Cu anode, and a scanning rate of 10°/min. To ascertain the final chemical structure of the doped samples, Fourier-transform infrared spectroscopy (FT-IR, Nicolet iS50, USA) and Raman spectroscopy (Renishaw inVia, Germany) were utilized. The morphology and elemental analysis of the doped samples were studied using a scanning electron microscope (SEM, JSM-5600LV, Japan) coupled with an energy-dispersive X-ray spectroscopy (EDS). For quantitative elemental analysis, approximately 3 mg of the dried samples were subjected to a Thermo Scientific elemental analyzer (Flash smart CHNS, Italy), and the atomic percentages of nitrogen, carbon, hydrogen, and sulfur were determined. The microwave absorption measurements were performed using a vector network analyzer (VNA) (Agilent-N5227A, USA).

3. Results and Discussions

3.1. *Physicochemical characterization of doped samples*

The XRD Phase patterns for NS-rGO are depicted in Fig. 2. The patterns display a broad and wide peak, centered at 24.4°, spanning from 20° to 33°. This can be attributed to the slightly larger interlayer spacing of the (002) diffraction planes of amorphous carbons, which is likely the result of the nitrogen and sulfur doping. Moreover, a clear peak can be observed at $2\theta = \sim 25.3°$ in the XRD pattern of neat CNTs (refer to Fig. S1). However, the pattern of NS-OCNT shows a diminished intensity of the (002) peak compared to the neat CNTs. This could be attributed to the disruption of the graphite structure caused by the insertion of the doping elements, N, and S.[49]

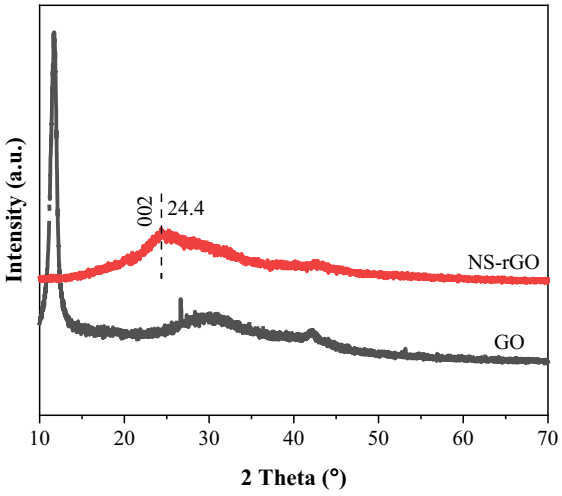

Fig. 2. XRD pattern for the sample of as-prepared GO and dual-doped rGO.

FT-IR spectra of the graphene oxide in Fig. 3(a), GO sample shows wide and strong peaks at about 3314 cm^{-1} corresponding to the stretching vibration of the O−H bond, due to the adsorbed H_2O molecules on GO.[50] Other absorption bands are noted between 2800 cm^{-1} and 3200 cm^{-1} representing the hydroxyl group in GO network.[51] Another strong peak at around 1021 cm^{-1} is also observed corresponding to C–O–C (epoxy) groups.[51] The intensities of these peaks reduced after the hydrothermal treatment demonstrated the doing of heteroatoms. Besides, a characteristic peak at 1448 cm^{-1} corresponding to the carboxyl group is

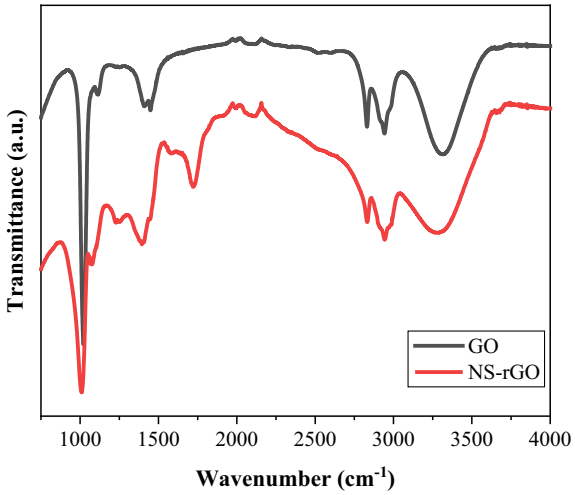

(a)

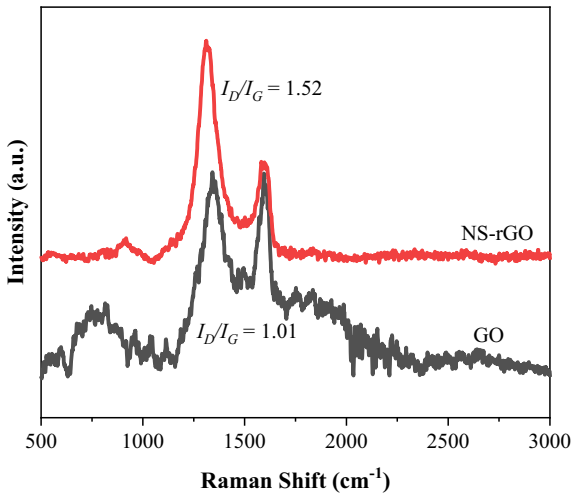

(b)

Fig. 3. (a) FTIR spectra for the sample of as-prepared GO and dual-doped rGO (b) Raman spectra for the sample of GO and dual-doped rGO.

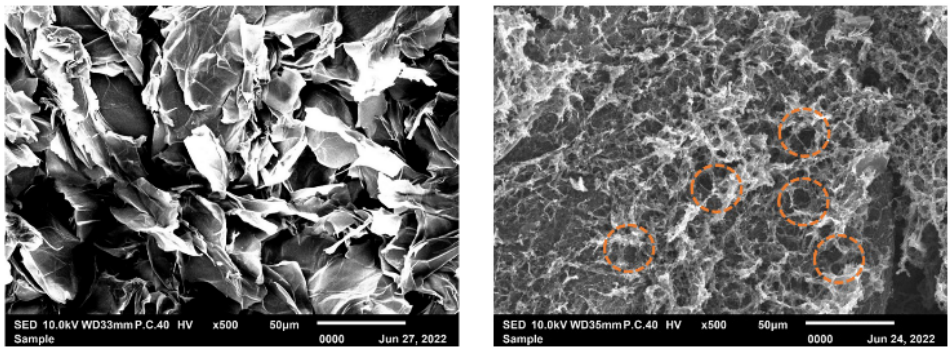

(a) (b)

Fig. 4. SEM images of as-prepared (a) GO and (b) NS-rGO.

also observed. After reacting with l-cysteine and thiourea for 16 h, this peak disappeared or shifted to a lower wavenumber (∼1394), indicating the insertion of N element.[52] Two absorption peaks at 1576 cm^{-1} and 1720 cm^{-1} were noted on the NS-rGO sample representing the vibrations of C = C, C = N, and C = O.[53] More importantly, the insertion of the S element is confirmed based on the feature of an absorption peak around 1200 cm^{-1} which is ascribed to the stretching vibration of a C−S,[53] and peak at 1075 cm^{-1} that corresponded to stretching vibrations of S = O bond in graphene sheet.[52]

Raman spectroscopy provides additional insights into the sulfur-co-nitrogen functionalization of rGO. As shown in Fig. 3(b), the Raman spectra of both GO and NS-rGO exhibit two prominent peaks near 1340 cm^{-1} and 1580 cm^{-1}. These peaks correspond to the corresponding to the D band, which arises from structural defects, and the G band, originating from the sp2-bonded graphitic carbon atoms, respectively. Generally, a higher intensity of the *D* band compared to the G band signifies a higher degree of disorder within the carbon material. The sample GO shows a peak at approximately 2640 cm^{-1} that is related to the second-order two-phonon mode 2D-band and is caused by the disordered property of carbon material.[54] The NS-rGO sample eliminated this peak. The G band of NS-rGO is slightly displaced to higher wavenumbers (approximately 10 cm^{-1}) than that of GO, which can be attributed to the development of p-type doped graphene. This phenomenon has also been observed in the literature and may be caused by the displacement of dopants in graphene sheets.[55]

Moreover, the ratios of the *D* to *G* peak intensities (I_D/I_G) are often used to estimate the level of defects in synthetic materials. For GO and NS-rGO, these ratios are observed to be 1.52 and 1.01, respectively, while the NS-OCNT exhibits an (I_D/I_G) ratio of 1.23 (refer to Fig. S2).

These findings suggest a higher number of structural defects in NS-rGO compared to both GO and NS-OCNT, which can be attributed to a high level of heteroatom doping.[56,57] Overall, the results from both XRD and Raman spectroscopy collectively indicate that the proposed material has been successfully doped with nitrogen and sulfur through a one-step hydrothermal process.

Figure 4 displays the morphological observation of GO samples before and after hydrothermal treatment. Figure 4(a) presents the morphology of pure GO, which is characteristically composed of stacked and interlaced ultrathin nanosheets.[58] In contrast, Fig. 4(b) depicts that NS-rGO foams composed of closely cross-linked graphene sheets that form a looser, porous 3D network.[54] This network is characterized by spherical holes, remnants of air bubbles, which pile on top of each other and are evenly distributed throughout the foam framework. It is suggested that this 3D porous network structure could enhance microwave absorption. The microporous framework inside the material can cause electromagnetic waves to repeatedly reflect off the walls in each individual closed void. Concurrently, the conductive network greatly enables the movement of electrons, leading to energy loss of the electromagnetic waves.[27] Actually, the conductivity of rGO increases from 12.65 μS to 174.70 μS in methanol medium and 25.40 μS to 72.35 μS in Distilled Water (DI) in our case (measured by standard conductivity meter probe) by incorporating dopant elements (see Table 1).

EDS mapping images, as displayed in Fig. S3, unambiguously demonstrate the presence of C, oxygen (O), and S elements. These elements are uniformly distributed across the field of view, which confirms the structural integrity of the 3D graphene network after treatment. These observations suggest successful sulfur functionalization of rGO.

Nitrogen, on the other hand, is not detected by SEM-EDX. This is likely due to the fact that nitrogen tends to have a very

Table 1. Electrical conductivity for the dual-doped sample.

Samples	Solvent	Conductivity (μS)
rGO	Methanol	12.65
	DI	25.40
NS-rGO	Methanol	174.70
	DI	72.35

Table 2. Elemental content for the dual-doped sample.

	Element %			
Sample name	Carbon	Hydrogen	Nitrogen	Sulfur
GO	44.69	3.09	0.09	1.06
NS-rGO	39.78	3.09	8.93	13.19

faint response, making its detection unreliable in most materials.[59] The results from CHNS analysis confirm the dual incorporation of S and N elements in rGO foams. As seen in Table 2, the NS-rGO sample exhibits a lower C content than the untreated GO sample, but it has higher N and S contents, which are 8.93% and 13.19%, respectively. This verifies successful heteroatom doping.

3.2. *Electromagnetic characterization of polymer-based nanocomposites filled with NS-rGO foams*

To study the effects of heteroatom doping, variations in the amount of the modified fillers, and the influence of pore structure on the microwave absorption properties and EMI shielding performance of the synthesized nanocomposites, two different loading amounts of NS-rGO in the PES matrix were used, namely, 0.2 wt.% and 0.5 wt.%.

The scattering parameters, S_{11} (reflection) and S_{21} (transmission) were measured across a frequency range of 8 to 12 GHz. The reflection coefficient (R) and transmission coefficient (T), as well as the EMI shielding effectiveness (SE), the absorption shielding effectiveness (SE_A), and the reflection shielding effectiveness (SE_R) of the nanocomposites can be computed from the scattering parameters (S_{11} and S_{21}, or S_{12} and S_{22}) using the following equations[60,61]:

$$R = |S_{11}|^2 = |S_{22}|^2, \tag{1}$$

$$T = |S_{21}|^2 = |S_{12}|^2, \tag{2}$$

$$\begin{aligned} SE_R &= -10\log(1-R) \\ &= 10\log\left(\frac{1}{1-R}\right) \\ &= 10\log\left(\frac{1}{1-|S_{11}|^2}\right). \end{aligned} \tag{3}$$

$$\begin{aligned} SE_A &= -10\log\left(\frac{T}{1-R}\right) \\ &= 10\log\left(\frac{1-R}{T}\right) \\ &= 10\log\left(\frac{1-|S_{11}|^2}{|S_{21}|^2}\right). \end{aligned} \tag{4}$$

$$SE = SE_R + SE_A = 10\log\frac{1}{T} = 10\log\left(\frac{1}{|S_{21}|^2}\right). \tag{5}$$

Figure 5(a) illustrates the transmission spectra of nanocomposite film. It is observed that compared to the control sample (GO@PES1), the doped samples exhibit a wider transmission window or bandpass feature at low frequencies. This finding suggests that the hydrothermal doping of GO significantly affects the electromagnetic response of the nanocomposites. Notably, lower transmission magnitude is exhibited by the NS-rGO@PES3 sample, suggesting its optimal doping capacity. Figure 5(b) shows that the total SE decreases at low frequencies and then increases after 9 GHz. This increase is typically associated with a polarization process occurring in the interfacial region due to the presence of a heterogeneous interface, characteristic of a one-phase heterostructure of rGO fillers.[62]

From the results, the SE values for GO@PES1, NS-rGO@PES2, and NS-rGO@PES3 were found to be 38 dB, 54 dB, and 60 dB, respectively, at a thickness of 3 mm.

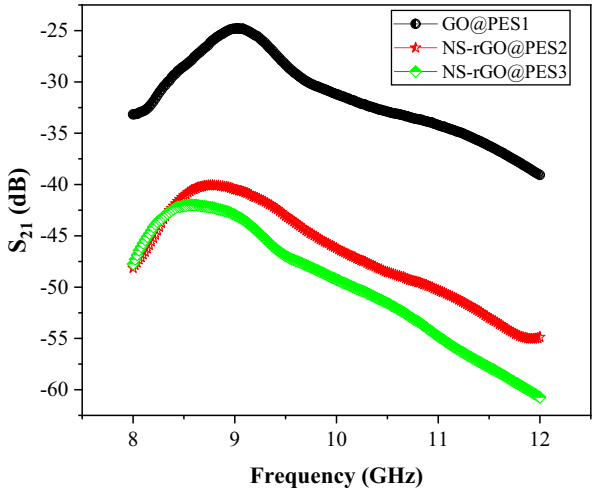

(a)

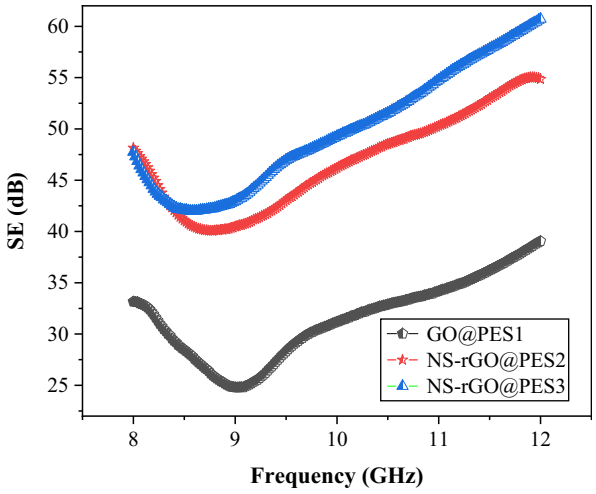

(b)

Fig. 5. (a) Transmission spectra S_{21} and (b) shielding effectiveness (SE) for the nanocomposite films.

In contrast, a nanocomposite fabricated from NS-OCNT with 0.5% loading exhibited an SE of about 45 dB (refer to Fig. S3). Remarkably, the NS-rGO@PES3 sample, which has an rGO loading amount of 0.5 wt.% demonstrates the optimal SE that is 25% higher than that of the NS-OCNT@PES4 nanocomposite with a similar loading amount. This suggests that the enhancement of the SE with optimal loading is attributable to the synergistic effects of S and N dual-doping and the reduction of GO in the hydrothermal process. Moreover, the pores present in the porous foams could enable multi-level reflections of the EM wave within the material, thus resulting in improved EMI shielding performance.[63] The electromagnetic shielding performance of a nanocomposite film (is generally accomplished via microwave absorption and/or reflection. For reflection-based shielding to occur, the material must contain movable charge carriers, such as electrons or holes, which are capable of interacting with the incident electromagnetic waves. Materials with high permeability can enhance absorption-based shielding.[62]

Interfacial polarization, stemming from disparities in permittivity, conductivity, and relaxation time of charge carriers across the interface, can result in significant SE from both absorption and reflections.[60] Indeed, the shielding performance achieved through absorption is intensified due to the nitrogen/sulfur doping of rGO. This doping process modulates the electrical and magnetic characteristics of the material, thus enhancing its shielding capabilities.[62] Moreover, the reduction that occurs during the treatment also plays a significant role in the high absorption performance of the nanocomposite. Reduced GO, produced during the hydrothermal process, is a superior option for microwave absorption compared to graphene and GO.[38]

The frequency-dependent electromagnetic parameters of the nanocomposite film samples are displayed in Fig. 6. There was only a slight change noted in the frequency range of 8.5–11 GHz. The optimum value of real permittivity (ε') was achieved by NS-rGO@PES3, which exhibits a notable peak value of 2.3 at around 9.12 GHz. The increase in the dielectric constant can be attributed to influences such as the Maxwell–Wagner–Sillars (MWS) polarization or interfacial polarization.[64] According to Debye's theory, the permittivity of free space (ε_0) and imaginary permittivity (ε'') follows the equation below[65]:

$$\varepsilon'' = \varepsilon_p'' + \varepsilon_c'' = (\varepsilon_s - \varepsilon_\infty)\frac{2\pi f\tau}{1+(2\pi f)^2} + \frac{\sigma}{2\pi f\varepsilon_0}. \quad (6)$$

Herein, ε_p'' and ε_c'' are the polarization relaxation and conductive loss. ε_s, ε_∞, f, τ, and σ represent the static permittivity, relative permittivity at the high-frequency limit, frequency, relaxation time, and electrical conductivity, respectively. As per the above equation, the ε'' is closely related to the ε_p'' and ε_c'' of nanocomposite samples.

From Eq. (6), the ε_c'' should decrease with increasing frequency. However, as shown in Fig. 6(a), an increase in the value of ε'' can be noted in the frequency range of 9–12 GHz. This increase could be attributed to the strong polarization relaxation in the resulting nanocomposites.[66] On the basis of the free electron theory, it can be deduced that the higher the electrical conductivity, the higher the ε'' specimen will have.[67]

Therefore, the NS-rGO@PES3 displays slightly larger ε' and ε'', indicating the improved storage capability of electric energy and dielectric loss.[67] Besides, negative values of ε'' were observed at low frequencies, while altered to positive for both NS-rGO@PES2 and NS-rGO@PES3 samples when the frequency reached 11.70 GHz. The phenomenon of positive ε' and negative ε'' was also reported in the literature.[68] Generally, the term metacomposites" refers to nanocomposites with the

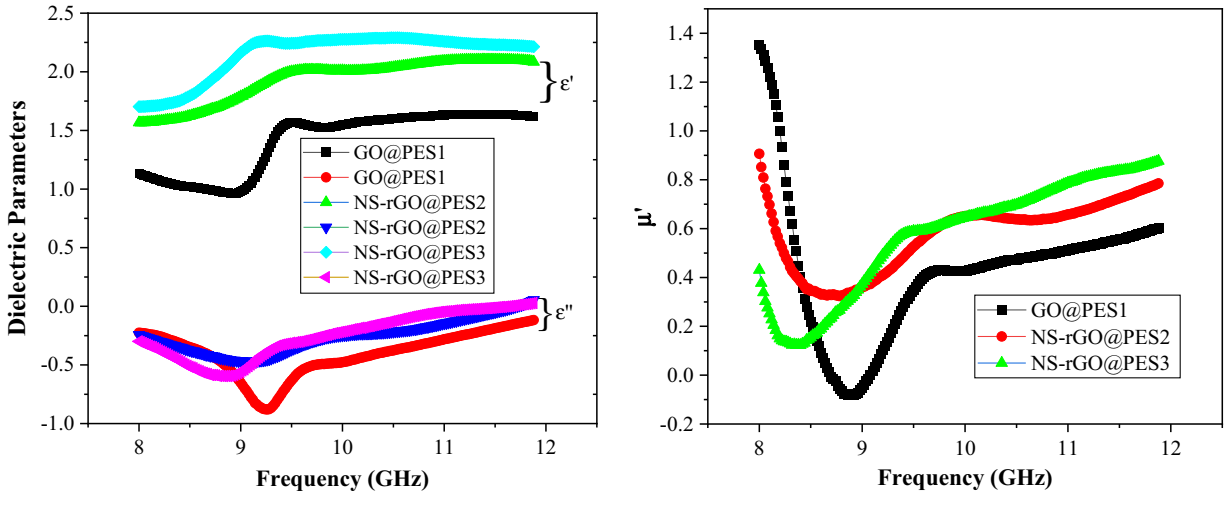

(a) (b)

Fig. 6. Frequency dispersion characteristics of (a) real permittivity and imaginary permittivity and (b) real part of permeability of the nanocomposite films.

unique characteristic of negative permittivity. This property depends on the loading, the frequency, and the nanofillers' morphology, and can be adjusted by altering these factors. Metacomposites have a wide range of potential applications, such as super lenses, wave filters, remote aerospace applications, and superconductors. In addition, the negative permittivity in the graphene nanocomposites could be assigned to the unique electronic energy dispersions (also known as surface plasmons). The positive permittivity may be due to the low plasmon resonance conductivity at a relatively high frequency.[69] This finding suggests that NS-rGO@PES2 and NS-rGO@PES3 samples have better conductivity than GO@PES1, because of the removal of most oxygen-containing groups, demonstrating the major influence of doping treatment on the EM shielding efficiency.[39] Thus, the conductivity of doped GO has a strong influence on its dielectric properties, which is consistent with the results presented in Table 1.

As shown in Fig. 6(b), all samples exhibit a slight decreasing trend in the real part of permeability (μ') at low frequency, with notable peaks observed between 8 and 9.50 GHz.

Attenuation loss, which includes dielectric loss and magnetic loss, is critical for microwave absorption. The dielectric loss tangent ($\tan\delta_\varepsilon = \varepsilon''/\varepsilon'$) and magnetic loss tangent ($\tan\delta_\mu = \mu''/\mu'$) can be utilized to estimate the dielectric loss and magnetic loss capacity of microwave absorbers. As shown in Fig. 7, the NS-rGO@PES2 and NS-rGO@PES3 samples demonstrate better $\tan\delta_\varepsilon$ compared to NS-GO@PES1, suggesting their enhanced dielectric loss against the incident microwaves. This enhancement can be linked with the occurrence of interfacial polarization, as a small amount of electron tunneling can occur.[70] In fact, heteroatoms and other sort of defects in graphene sheets like the remaining oxygen-containing groups as well as restacking of graphene layers that are likely to occur during the reduction process can serve as a polarization center to elevate the material loss, hence dissipate microwave energy.[39]

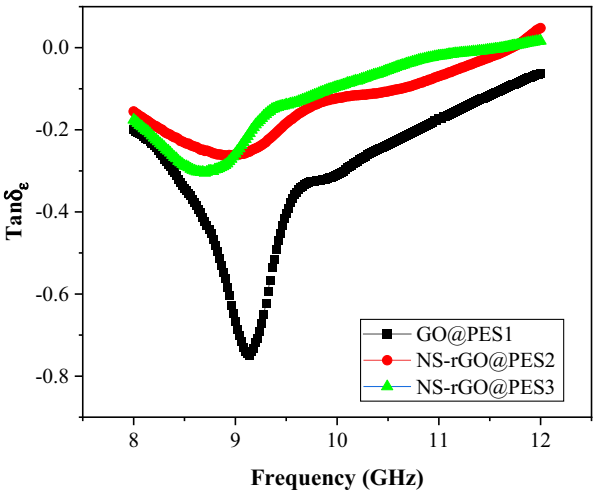

Fig. 7. Frequency dispersion characteristics of dielectric loss tangent of the nanocomposite films.

4. Conclusion

The nitrogen-co-sulfur-doped reduced graphene-oxide (NS-rGO) films with 3D porous structures were synthesized through a hydrothermal method, employing l-cysteine and thiourea as doping precursors. Subsequently, nanocomposite films were fabricated by incorporating the NS-rGO foams into polyethersulfone (PES) through the hot-pressing technique. The examination of elemental content confirmed the successful insertion of sulfur and nitrogen functionalities into rGO. The microwave characterization of the resulting shielding film demonstrated excellent electromagnetic interference shielding performance, which can be attributed to the existence of the porous structure and the heteroatom insertion. The highest shielding effectiveness was achieved at the loading of 0.5 wt.% of NS-rGO. Overall, this work provides guidance for the functional composites and the engineering of pore structures in carbon nanomaterials. The proposed material exhibits great potential for applications in microwave absorption. This type of microwave absorption material represents a favorable solution for environmental protection in the field of EMI shielding.

Acknowledgments

The authors gratefully acknowledge the support and funding provided by the postdoctoral scholarship research program of the Islamic Development Bank (IsDB), KSA (Grant No. 600040856) and the project of Prof. Md Zahangir Alam, Kulliyyah of engineering, (IIUM) (Grant No. RC-RIGS20-004-0004).

Supplementary Material

The Supplementary Material is available at: https://www.worldscientific.com/doi/suppl/10.1142/S2010135X23500297

ORCID

Tienah H. H. Elagib https://orcid.org/0000-0003-2473-9806
Nassereldeen A. Kabbashi https://orcid.org/0000-0002-1524-5065
Md Zahangir Alam https://orcid.org/0000-0002-6491-3218
Elwathig A. M. Hassan https://orcid.org/0000-0002-8917-0481
Mohamed E. S. Mirghani https://orcid.org/0000-0002-9558-9449
Nour Hamid Abdurahman https://orcid.org/0000-0002-7269-3761

References

[1]Q. Wang, B. Niu, Y. Han, Q. Zheng, L. Li and M. Cao, Nature-inspired 3D hierarchical structured "vine" for efficient microwave

attenuation and electromagnetic energy conversion device, *Chem. Eng. J.* **452**, 139042 (2023).
[2]Q. Zheng, J. Wang, M. Yu, W.-Q. Cao, H. Zhai and M.-S. Cao, Heterodimensional structure porous nanofibers embedded confining magnetic nanocrystals for electromagnetic functional material and device, *Carbon* **210**, 118049 (2023).
[3]X. Ma, J. Pan, H. Guo, J. Wang, C. Zhang, J. Han, Z. Lou, C. Ma, S. Jiang and K. Zhang, Ultrathin wood-derived conductive carbon composite film for electromagnetic shielding and electric heating management, *Adv. Funct. Mater.* **33**, 2213431 (2023).
[4]Y.-Y. Wang, W.-J. Sun, D.-X. Yan, K. Dai and Z.-M. Li, Ultralight carbon nanotube/graphene/polyimide foam with heterogeneous interfaces for efficient electromagnetic interference shielding and electromagnetic wave absorption, *Carbon* **176**, 118 (2021).
[5]Y. Wang, Z.-W. Fan, H. Zhang, J. Guo, D.-X. Yan, S. Wang, K. Dai and Z.-M. Li, 3D-printing of segregated carbon nanotube/polylactic acid composite with enhanced electromagnetic interference shielding and mechanical performance, *Mater. Des.* **197**, 109222 (2021).
[6]C. Li, H. Zhang, Y. Song, L. Cai, J. Wu, J. Wu, S. Wang and C. Xiong, Robust superhydrophobic and porous melamine-formaldehyde based composites for high-performance electromagnetic interference shielding, *Colloids Surf. A* **624**, 126742 (2021).
[7]W.-C. Yu, T. Wang, G.-Q. Zhang, Z.-G. Wang, H.-M. Yin, D.-X. Yan, J.-Z. Xu and Z.-M. Li, Largely enhanced mechanical property of segregated carbon nanotube/poly (vinylidene fluoride) composites with high electromagnetic interference shielding performance, *Compos. Sci. Technol.* **167**, 260 (2018).
[8]J. Ju, T. Kuang, X. Ke, M. Zeng, Z. Chen, S. Zhang and X. Peng, Lightweight multifunctional polypropylene/carbon nanotubes/carbon black nanocomposite foams with segregated structure, ultralow percolation threshold and enhanced electromagnetic interference shielding performance, *Compos. Sci. Technol.* **193**, 108116 (2020).
[9]H.-Y. Zhang, J.-Y. Li, Y. Pan, Y.-F. Liu, N. Mahmood and X. Jian, Flexible carbon fiber-based composites for electromagnetic interference shielding, *Rare Met.* **41**, 1 (2022).
[10]T. Sun, Z. Liu, S. Li, H. Liu, F. Chen, K. Wang and Y. Zhao, Effective improvement on microwave absorbing performance of epoxy resin-based composites with 3D MXene foam prepared by one-step impregnation method, *Compos. A* **150**, 106594 (2021).
[11]K. Zubair, A. Ashraf, H. Gulzar, M. F. Shakir, Y. Nawab, Z. Rehan and I. A. Rashid, Study of mechanical, electrical and EMI shielding properties of polymer-based nanocomposites incorporating polyaniline coated graphene nanoparticles, *Nano Express* **2**, 010038 (2021).
[12]W. Cai, W. Ma, W. Chen, P. Liu, Y. Liu, Z. Liu, W. He and J. Li, Microwave-assisted reduction and sintering to construct hybrid networks of reduced graphene oxide and MXene for electromagnetic interference shielding, *Compos. A* **157**, 106928 (2022).
[13]H. K. Choudhary, R. Kumar, S. P. Pawar and B. Sahoo, Role of graphitization-controlled conductivity in enhancing absorption dominated EMI shielding behavior of pyrolysis-derived Fe3C@C-PVDF nanocomposites, *Mater. Chem. Phys.* **263**, 124429 (2021).
[14]J. Kruželák, A. Kvasničáková, K. Hložeková and I. Hudec, Progress in polymers and polymer composites used as efficient materials for EMI shielding, *Nanoscale Adv.* **3**, 123 (2021).
[15]H. K. Choudhary, R. Kumar, S. P. Pawar, U. Sundararaj and B. Sahoo, Superiority of graphite coated metallic-nanoparticles over graphite coated insulating-nanoparticles for enhancing EMI shielding, *New J. Chem.* **45**, 4592 (2021).
[16]K. Sushmita, P. Formanek, B. Krause, P. Po¨tschke and S. Bose, Distribution of carbon nanotubes in polycarbonate-based blends for electromagnetic interference shielding, *ACS Appl. Nano Mater.* **5**, 662 (2022).
[17]K. S. Kumar, R. Rengaraj, G. Venkatakrishnan and A. Chandramohan, Polymeric materials for electromagnetic shielding-A review, *Mater. Today Proc.* **47**, 4925 (2021).
[18]Y. Wang, X. Gao, Y. Fu, X. Wu, Q. Wang, W. Zhang and C. Luo, Enhanced microwave absorption performances of polyaniline/graphene aerogel by covalent bonding, *Compos. B* **169**, 221 (2019).
[19]Y. Chen, J. Li, T. Li, L. Zhang and F. Meng, Recent advances in graphene-based films for electromagnetic interference shielding: Review and future prospects, *Carbon* **180**, 163 (2021).
[20]P. Song, C. Liang, L. Wang, H. Qiu, H. Gu, J. Kong and J. Gu, Obviously improved electromagnetic interference shielding performances for epoxy composites via constructing honeycomb structural reduced graphene oxide, *Compos. Sci. Technol.* **181**, 107698 (2019).
[21]F. Sharif, M. Arjmand, A. A. Moud, U. Sundararaj and E. P. Roberts, Segregated hybrid poly (methyl methacrylate)/graphene/magnetite nanocomposites for electromagnetic interference shielding, *ACS Appl. Mater. Interfaces* **9**, 14171 (2017).
[22]K. Zhang, G.-H. Li, L.-M. Feng, N. Wang, J. Guo, K. Sun, K.-X. Yu, J.-B. Zeng, T. Li and Z. Guo, Ultralow percolation threshold and enhanced electromagnetic interference shielding in poly (L-lactide)/multi-walled carbon nanotube nanocomposites with electrically conductive segregated networks, *J. Mater. Chem. C* **5**, 9359 (2017).
[23]Y. Wu, Z. Wang, X. Liu, X. Shen, Q. Zheng, Q. Xue and J.-K. Kim, Ultralight graphene foam/conductive polymer composites for exceptional electromagnetic interference shielding, *ACS Appl. Mater. Interfaces* **9**, 9059 (2017).
[24]C. Liang, H. Qiu, Y. Han, H. Gu, P. Song, L. Wang, J. Kong, D. Cao and J. Gu, Superior electromagnetic interference shielding 3D graphene nanoplatelets/reduced graphene oxide foam/epoxy nanocomposites with high thermal conductivity, *Mater. Chem. C* **7**, 2725 (2019).
[25]H. Liu, Y. Xu, J.-P. Cao, D. Han, Q. Yang, R. Li and F. Zhao, Skin structured silver/three-dimensional graphene/polydimethylsiloxane composites with exceptional electromagnetic interference shielding effectiveness, *Compos. A* **148**, 106476 (2021).
[26]S.-H. Lee, D. Kang and I.-K. Oh, Multilayered graphene-carbon nanotube-iron oxide three-dimensional heterostructure for flexible electromagnetic interference shielding film, *Carbon* **111**, 248 (2017).
[27]J. Li, X. Zhao, W. Wu, X. Ji, Y. Lu and L. Zhang, Bubble-templated rGO-graphene nanoplatelet foams encapsulated in silicon rubber for electromagnetic interference shielding and high thermal conductivity, *Chem. Eng. J* **415**, 129054 (2021).
[28]J. Chen, X. Liang, W. Liu, W. Gu, B. Zhang and G. Ji, Mesoporous carbon hollow spheres as a light weight microwave absorbing material showing modulating dielectric loss, *Dalton Trans.* **48**, 10145 (2019).
[29]X. Qiu, L. Wang, H. Zhu, Y. Guan and Q. Zhang, Lightweight and efficient microwave absorbing materials based on walnut shell-derived nano-porous carbon, *Nanoscale* **9**, 7408 (2017).

[30]Y. Yang, M. C. Gupta, K. L. Dudley and R. W. Lawrence, Novel carbon nanotube – polystyrene foam composites for electromagnetic interference shielding, *Nano Lett.* **5**, 2131 (2005).
[31]J. Chen, X. Liao, S. Li, W. Wang, F. Guo and G. Li, A promising strategy for efficient electromagnetic interference shielding by designing a porous double-percolated structure in MWCNT/polymer-based composites, *Compos. A* **138**, 106059 (2020).
[32]J.-M. Thomassin, C. Pagnoulle, L. Bednarz, I. Huynen, R. Jerome and C. Detrembleur, Foams of polycaprolactone/MWNT nanocomposites for efficient EMI reduction, *J. Mater. Chem.* **18**, 792 (2008).
[33]X.-Y. Wang, S.-Y. Liao, H.-P. Huang, Y.-G. Hu, P.-L. Zhu, R. Sun and Y.-J. Wan, graphene oxide/carbon tube composite films with tunable porous structures for electromagnetic interference shielding, *ACS Appl. Nano Mater.* **5**, 13509 (2022).
[34]J. Tang, N. Liang, L. Wang, J. Li, G. Tian, D. Zhang, S. Feng and H. Yue, Three-dimensional nitrogen-doped reduced graphene oxide aerogel decorated with Ni nanoparticles with tunable and unique microwave absorption, *Carbon* **152**, 575 (2019).
[35]F. Banhart, J. Kotakoski and A. V. Krasheninnikov, Structural defects in graphene, *ACS Nano* **5**, 26 (2011).
[36]B. Quan, X. Liang, G. Ji, Y. Cheng, W. Liu, J. Ma, Y. Zhang, D. Li and G. Xu, Dielectric polarization in electromagnetic wave absorption: Review and perspective, *J. Alloys Compd.* **728**, 1065 (2017).
[37]Y. Qing, Y. Li and F. Luo, Electromagnetic interference shielding properties of nitrogen-doped graphene/epoxy composites, *J. Mater. Sci.: Mater. Electron.* **32**, 25649 (2021).
[38]L. Quan, F. Qin, D. Estevez, H. Wang and H. Peng, Magnetic graphene for microwave absorbing application: towards the lightest graphene-based absorber, *Carbon* **125**, 630 (2017).
[39]Q. Li, X. Tian, W. Yang, L. Hou, Y. Li, B. Jiang, X. Wang and Y. Li, Fabrication of porous graphene-like carbon nanosheets with rich doped-nitrogen for high-performance electromagnetic microwave absorption, *Appl. Surf. Sci.* **530**, 147298 (2020).
[40]L. Quan, F. Qin, Y. Li, D. Estevez, G. Fu, H. Wang and H. Peng, Magnetic graphene enabled tunable microwave absorber via thermal control, *Nanotechnology* **29**, 245706 (2018).
[41]J. Tuček, P. Błoński, Z. Sofer, P. Šimek, M. Petr, M. Pumera, M. Otyepka and R. Zbořil, Sulfur doping induces strong ferromagnetic ordering in graphene: Effect of concentration and substitution mechanism, *Adv. Mater.* **28**, 5045 (2016).
[42]J. Feng, F. Pu, Z. Li, X. Li, X. Hu and J. Bai, Interfacial interactions and synergistic effect of CoNi nanocrystals and nitrogen-doped graphene in a composite microwave absorber, *Carbon* **104**, 214 (2016).
[43]Z. Li, X. Li, Y. Zong, G. Tan, Y. Sun, Y. Lan, M. He, Z. Ren and X. Zheng, Solvothermal synthesis of nitrogen-doped graphene decorated by superparamagnetic Fe3O4 nanoparticles and their applications as enhanced synergistic microwave absorbers, *Carbon* **115**, 493 (2017).
[44]R. Sánchez-Salas, E. Muñoz-Sandoval, M. Endo, A. Morelos-Gómez and F. López-Urías, Nitrogen and sulfur incorporation into graphene oxide by mechanical process, *Adv. Eng. Mater.* **23**, 2001444 (2021).
[45]P. Sun, H. Liu, M. Feng, L. Guo, Z. Zhai, Y. Fang, X. Zhang and V. K. Sharma, Nitrogen-sulfur co-doped industrial graphene as an efficient peroxymonosulfate activator: Singlet oxygen-dominated catalytic degradation of organic contaminants, *Appl. Catal., B* **251**, 335 (2019).
[46]V. Thirumal, T. Sreekanth, K. Yoo and J. Kim, Biomass-derived hard carbon and nitrogen-sulfur co-doped graphene for high-performance symmetric sodium ion capacitor devices, *Energies* **16**, 802 (2023).
[47]M. F. Gasim, A. Veksha, G. Lisak, S.-C. Low, T. S. Hamidon, M. H. Hussin and W.-D. Oh, Importance of carbon structure for nitrogen and sulfur co-doping to promote superior ciprofloxacin removal via peroxymonosulfate activation, *J. Colloid Interface Sci.* **634**, 586 (2023).
[48]T. H. Elagib, N. A. Kabbashi, M. Z. Alam, M. E. Mirghani and E. A. Hassan, The performance of heteroatom-doped carbon nanotubes synthesized via a hydrothermal method on the oxygen reduction reaction and specific capacitance: Original scientific paper, *J. Electrochem. Sci. Technol. Eng.* (2023), DOI: 10.5599/jese.1697.
[49]J. Zhao, Y. Liu, X. Quan, S. Chen, H. Zhao and H. Yu, Nitrogen and sulfur co-doped graphene/carbon nanotube as metal-free electrocatalyst for oxygen evolution reaction: the enhanced performance by sulfur doping, *Electrochim. Acta* **204**, 169 (2016).
[50]S. N. Alam, N. Sharma and L. Kumar, Synthesis of graphene oxide (GO) by modified hummers method and its thermal reduction to obtain reduced graphene oxide (rGO), *Graphene* **6**, 1 (2017).
[51]N. I. Zaaba, K. L. Foo, U. Hashim, S. J. Tan, W.-W. Liu and C. H. Voon, Synthesis of graphene oxide using modified hummers method: solvent influence, *Procedia Eng.* **184**, 469 (2017).
[52]B.-X. Zhang, H. Gao and X.-L. Li, Synthesis and optical properties of nitrogen and sulfur co-doped graphene quantum dots, *New J. Chem.* **38**, 4615 (2014).
[53]Z. S. Schroer, Y. Wu, Y. Xing, X. Wu, X. Liu, X. Wang, O. G. Pino, C. Zhou, C. Combs and Q. Pu, Nitrogen–sulfur-doped graphene quantum dots with metal ion-resistance for bioimaging, *ACS Appl. Nano Mater.* **2**, 6858 (2019).
[54]D. Wu, T. Wang, L. Wang and D. Jia, Hydrothermal synthesis of nitrogen, sulfur co-doped graphene and its high performance in supercapacitor and oxygen reduction reaction, *Microporous Mesoporous Mater.* **290**, 109556 (2019).
[55]T. Wang, L. Wang, D. Wu, W. Xia, H. Zhao and D. Jia, Hydrothermal synthesis of nitrogen-doped graphene hydrogels using amino acids with different acidities as doping agents, *J. Mater. Chem. A* **2**, 8352 (2014).
[56]K. Kakaei and G. Ghadimi, A green method for Nitrogen-doped graphene and its application for oxygen reduction reaction in alkaline media, *Mater. Technol.* **36**, 46 (2021).
[57]G. Sun, H. Xie, J. Ran, L. Ma, X. Shen, J. Hu and H. Tong, Rational design of uniformly embedded metal oxide nanoparticles into nitrogen-doped carbon aerogel for high-performance asymmetric supercapacitors with a high operating voltage window, *J. Mater. Chem. A* **4**, 16576 (2016).
[58]J. Guo, S. Zhang, M. Zheng, J. Tang, L. Liu, J. Chen and X. Wang, Graphitic-N-rich N-doped graphene as a high performance catalyst for oxygen reduction reaction in alkaline solution, *Int. J. Hydrogen Energy* **45**, 32402 (2020).
[59]W. J. Wolfgong, *Handbook of Materials Failure Analysis with Case Studies from the Aerospace and Automotive Industries*, eds. A. S. H. Makhlouf and M. Aliofkhazraei, Chap. 14 (Butterworth-Heinemann, Boston, 2016), pp. 279–307.

[60]Y. Xu, A. Uddin, D. Estevez, Y. Luo, H. Peng and F. Qin, Lightweight microwire/graphene/silicone rubber composites for efficient electromagnetic interference shielding and low microwave reflectivity, *Compos. Sci. Technol.* **189**, 108022 (2020).

[61]T. Lu, H. Gu, Y. Hu, T. Zhao, P. Zhu, R. Sun and C.-P. Wong, Three dimensional copper foam-filled elastic conductive composites with simultaneously enhanced mechanical, electrical, thermal and electromagnetic interference (emi) shielding properties, *69th Electronic Components and Technology Conf.* (2019), pp. 1916–1920.

[62]T. H. Elagib, N. A. Kabbashi, E. A. Hassan, M. Alam and M. A. F. Al-Khatib, The role of high-performance microwave absorbing materials in electromagnetic interference shielding: A review of the advanced internal design of polymer-based nano-composites, *Ann. Faculty Eng. Hunedoara-Int. J. Eng.* 19 (2022).

[63]Y. Yu, Z. Chao, Q. Gong, C. Li, H. Fu, F. Lei, D. Hu and L. Zheng, Tailoring hierarchical carbon nanotube cellular structure for electromagnetic interference shielding in extreme conditions, *Mater. Des.* **206**, 109783 (2021).

[64]A. Ashery, A. Gaballah and E. M. Ahmed, Tuned high dielectric constant, low dielectric loss tangent with positive and negative values for PPy/MWCNTs/TiO2/Al2O3/n-Si, *J. Exp. Nanosci.* **16**, 309 (2021).

[65]R. Shu, Y. Wu, W. Li, J. Zhang, Y. Liu, J. Shi and M. Zheng, Fabrication of ferroferric oxide–carbon/reduced graphene oxide nanocomposites derived from Fe-based metal–organic frameworks for microwave absorption, *Compos. Sci. Technol.* **196**, 108240 (2020).

[66]R. Shu, G. Zhang, C. Zhang, Y. Wu and J. Zhang, Nitrogen-doping-regulated electromagnetic wave absorption properties of ultralight three-dimensional porous reduced graphene oxide aerogels, *Adv. Electron. Mater.* **7**, 2001001 (2021).

[67]Y. Wu, R. Shu, X. Shan, J. Zhang, J. Shi, Y. Liu and M. Zheng, Facile design of cubic-like cerium oxide nanoparticles decorated reduced graphene oxide with enhanced microwave absorption properties, *J. Alloys Compd.* **817**, 152766 (2020).

[68]X. Zhang, J. Zhu, N. Haldolaarachchige, J. Ryu, D. P. Young, S. Wei and Z. Guo, Synthetic process engineered polyaniline nanostructures with tunable morphology and physical properties, *Polymer* **53**, 2109 (2012).

[69]H. Gu, J. Guo, S. Wei and Z. Guo, Polyaniline nanocomposites with negative permittivity, *J. Appl. Polym. Sci.* **130**, 2238 (2013).

[70]P. Kum-onsa, N. Phromviyo and P. Thongbai, Na1/3Ca1/3Bi1/3$Cu_3Ti_4O_{12}$–Ni@ NiO/poly (vinylidene fluoride): Three–phase polymer composites with high dielectric permittivity and low loss tangent, *Results Phys.* **18**, 103312 (2020).